GDCh Research Article Angewandte International Edition Chemie www.angewandte.org

Check for updates

How to cite: *Angew. Chem. Int. Ed.* **2025**, *64*, e202516086
doi.org/10.1002/anie.202516086

Heterogeneous Catalysis

Mechanistic Insights into Adsorptive and Catalytic Reactions from Controllable Distributions of Metal Cations (Pd, Pt, Ni, Cr, Cu) as $[M\text{-}OH]^{+1}$/1Al or M^{+2}/2Al in Zeolites

Nicholas R. Jaegers[+], Miroslaw A. Derewinski,* Eric D. Walter, Iskra Z. Koleva, Daria Boglaienko, Dhruba J. Deka, Garam Lee, Trent R. Graham, Libor Kovarik, Yong Wang, Janos Szanyi, Hristiyan A. Aleksandrov,* and Konstantin Khivantsev[+]**

Abstract: Anchoring divalent metal ions in the same zeolite framework with similar Si/Al ratio selectively as zeolite-bound M^{+2} or $[M^{+2}\text{-}OH]^{+1}$ cationic species enables critical comparison of the species' intrinsic reactivity for industrially and fundamentally relevant reactions. H-BEA zeolites with similar Si/Al ratios but differing framework Al siting were used to anchored multiple divalent metal cations (Ni, Pd, Pt, Cr, Cu) in the zeolite micropores. State-of-the-art infrared (IR) spectroscopy, electron paramagnetic resonance (EPR) measurements, including two-dimensional pulsed HYSCORE EPR, extended X-ray absorption fine structure (EXAFS), and density functional theory (DFT) calculations together provide unambiguous evidence for the selective formation of divalent metal cations as M^{+2}/2Al species (for H-BEA prepared in the conventional hydroxide media), and $[M^{+2}OH]^{+1}$/1Al species for H-BEA prepared in HF. Solid-state proton-decoupled triple-quantum magic-angle spinning (3Q MAS) NMR measurements confirmed contrasting Al distributions in the two H-BEA zeolites, which led to a contrasting divalent cation speciation. The reactivities of the two cationic species were explored for catalytic and adsorptive applications in both organometallic homogeneous and heterogeneous catalysis. This work demonstrates their divergent reactivity in ethylene dimerization, ethylene oxidation (Wacker process), selective catalytic reduction (SCR) of NO, NO adsorption, and methane oxidation. Both M^{+2}/2Al and $[M^{+2}OH]^{+1}$/1Al cations are both active for ethylene dimerization, but $[M^{+2}OH]^{+1}$/1Al species show higher reaction rates for each Pd, Ni, Pt. $[M^{+2}OH]^{+1}$/1Al is active for acetaldehyde formation in Wacker ethylene oxidation. A new active site for ethylene oligomerization is proposed that possesses a terminal OH group (Cr-OH) in Phillips catalysts evident by a nearly inactive isolated Cr^{+2}/2Al species that contrast an active Cr—OH motif.

Introduction

Zeolite-supported transition metals are an important class of materials for catalysis, adsorption and as model systems for elucidation reaction mechanisms[1–5] This is due to the highly crystalline nature of zeolites and well-defined binding sites in their micropores. Metal cations such as Rh, Ir, Ni, Pt, Pd, and Cu have been introduced in zeolites and proved useful for various reactions: alkane activation, olefin di- and oligomerization, NO reduction/storage among others.[1–10]

The Al distribution in zeolites is important for reactivity and stability[11–16] as it must impact the anchoring of such metal species.[17] Methods to control the Al distribution, and thus, cation speciation with organic structure directing agents (SDAs) have been described,[13,14,16,18–36] leading to various Al site distributions. These distributions were probed with ^{27}Al solid-state nuclear magnetic resonance as well as by analysis of ^{23}Na and ^{7}Li nuclei. The presence of Al pairs (closely spaced Al framework atoms) is often assured with Co^{+2} ion titration, where Co ions are believed to be

[*] N. R. Jaegers[+]
Dept. of Chemical & Biological Engineering, University of New Mexico, Albuquerque, USA
E-mail: NJaegers@unm.edu

M. A. Derewinski, E. D. Walter, D. Boglaienko, D. J. Deka, G. Lee, T. R. Graham, L. Kovarik, Y. Wang, J. Szanyi, K. Khivantsev[+]
Pacific Northwest National Laboratory, Richland, WA 99352, USA
E-mail: Derewinski@gmail.com
Konstantin.Khivantsev@pnnl.gov

I. Z. Koleva, H. A. Aleksandrov
Faculty of Chemistry and Pharmacy, Sofia University "St. Kliment Ohridski", Sofia 1164, Bulgaria
E-mail: HAA@chem.uni-sofia.bg

H. A. Aleksandrov
Center of Excellence "Universities for Science, Informatics and Technologies in eSociety" (UNITe), Sofia 1164, Bulgaria

Y. Wang
Voiland School of Chemical Engineering and Bioengineering Institution, Washington State University, Pullman, Washington 99164, USA

[+] Both authors contributed equally to this work.

Additional supporting information can be found online in the Supporting Information section

adsorbed exclusively as Co^{+2} sites held by proximal Al pairs, i.e., M^{+2}/2Al. Recently, this simple assumption has been challenged.[37] However, little is known about what the exact state of catalytically relevant divalent metal cations (such as Pd, Pt, Ni, Cu, Cr) is in zeolites with different Al distributions (and whether it can be controlled) as the spectroscopic and analytical tools to assess such distribution are currently lacking. In general, divalent metal cations in zeolites can occupy ion exchange sites in zeolites as M^{+2}/2Al (when Al pairs are present) and/or $[M^{+2}OH]^{+1}$/1Al species (when isolated Al sites are present). To the best of our knowledge, there are no examples of selectively preparing one or the other type in the same zeolite with similar Si/Al ratio but different Al distribution.

The goal of this study was to selectively anchor divalent metal cations in the same zeolite with similar Si/Al ratio either as M^{+2}/2Al and $[M^{+2}OH]^{+1}$/1Al and develop spectroscopic and theoretical framework to pinpoint their signatures. We further aimed to elucidate the catalytic reactivity of the resulting materials in fundamentally and industrially important reactions, such as ethylene conversion to butenes (dimerization) and acetaldehyde (Wacker oxidation), selective catalytic reduction (SCR), nitric oxide adsorption, and methane oxidation, which has not been possible before.

Results and Discussion

Tunable Al Distribution Revealed by Nuclear Magnetic Resonance

We employed H-BEA zeolite: a zeolite with large pore opening (~7 Angstroms) and straight microporous channels (HRTEM images of H-BEA crystals shown in Figure S1) fully available to reacting molecules. We utilized BEA crystals with similar Si/Al ratios (~13–15) synthesized in the regular (hydroxide) and fluoride media (Surface areas summarized in Table S1; infrared spectra for H-BEA samples is shown in Figures S2 and S3).[38,39] 3QMAS NMR spectroscopy was used to show the ^{27}Al distribution in each sample (Figure 1). The 3QMAS NMR of each sample shows a highly symmetric feature at 58 ppm and a less symmetric environment at 62 ppm, both relating to tetrahedral Al species. Single-pulse ^{27}Al NMR measurements revealed at least two distinct tetrahedral sites in each sample with differing distributions and abundances. HBEA-OH peak intensities favoring resonance near 53.6 ppm, which likely correspond to the less-symmetric species while those of HBEA-F favor resonance at 57.3 ppm. The less-symmetric species may reflect distortion imparted by proximal defects, silanols, or event distortions from proximal Al species. These results are consistent structure-directing agents (fluoride versus OH) in the synthesis gel impacting contrasting Al distribution.

This prompted us to evaluate the state of divalent metal cations in these samples, with the expectation that different Al site distributions may lead to different divalent metal ionic sites. We loaded both samples with Pd (0.4–1 wt%). Probing Pd distribution with CO probe molecule and infrared spectroscopy reveals striking differences in Figure 2: Pd in

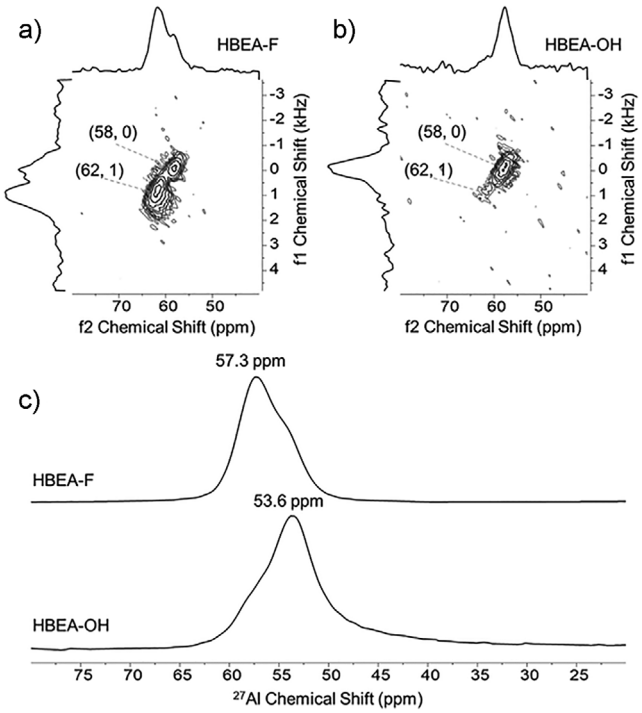

Figure 1. Proton-decoupled, triple quantum magic angle spinning (3QMAS) ^{27}Al NMR spectra showing the variation in tetrahedral Al speciation in the a) HBEA-F and b) HBEA-OH samples, as well as c) single pulse direct excitation ^{27}Al MAS NMR spectra.

zeolite H-BEA (OH) shows majority of Pd present as isolated, zeolite-anchored palladium ions (Pd^{+2}/2Al) with 2214 and 2193 cm^{-1} symmetric and asymmetric stretches belonging to Pd gem-dicarbonyl complexes $Pd^{+2}(CO)_2$ (Figure 2a).[10] However, Pd ions in H-BEA (fluoride) shows majorly 1 band with a center at 2127 cm^{-1} (Figure 2b). We will show below that this band belongs to $[Pd^{+2}(OH)(CO)]^{+1}$/1Al cationic species.

Importantly, we observed similar differences for Ni ions in zeolite H-BEA (Figure 2b,c). In the case of Ni, Ni^{+2} ions adsorb only 1 CO ligand,[40] unlike Pd^{+2} which forms dicarbonyls. However, Ni^{+2}/2Al can be distinguished from $[Ni^{+2}(OH)]^{+1}$/1Al through CO adsorption IR spectral measurements. Ni in H-BEA (OH) shows one high-lying band at 2211 cm^{-1}, whereas Ni in H-BEA (F) shows 1 band, significantly downshifted, at ~2125 cm^{-1}. Once again, qualitatively these results are analogous both for Pd and Ni cations in H-BEA zeolites: divalent M in B-BEA (F) shows a downshifted signature, in contrast to typical signatures of M^{+2}/2Al cations in H-BEA (OH).

Comparison of calculated and experimental C—O vibrational frequencies of the carbonyl complexes of M(II) and M(II)(OH) (M = Pd and Ni) cations located in the pores of BEA

We modeled different carbonyl complexes of Pd and Ni ions in BEA and compared those with our experimental data: $Pd^{+2}(CO)_2$/2Al, $[Pd^{+2}(OH)(CO)]^{+1}$/1Al, $Ni^{+2}(CO)$/2Al, and

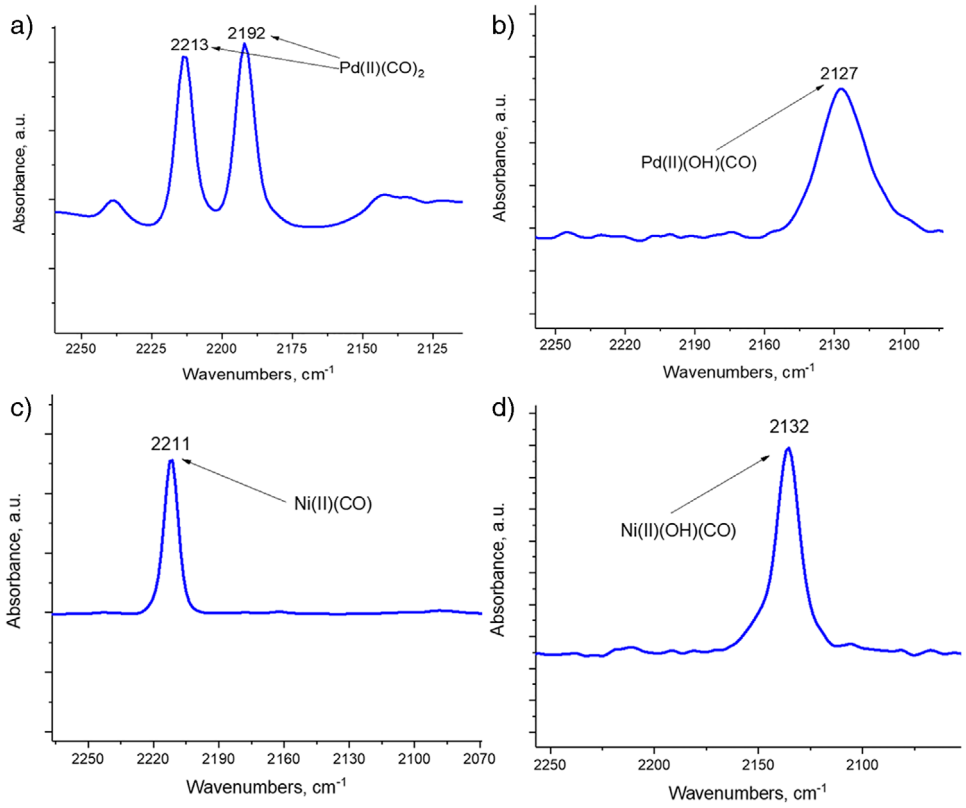

Figure 2. Infrared spectra after 2 Torr CO adsorption on a) 1 wt% Pd/H-BEA (OH), b) 1 wt% Pd/H-BEA (F), c) 0.4 wt% Ni/H-BEA (OH), and d) 0.4 wt% Ni/H-BEA (F) at 298 K.

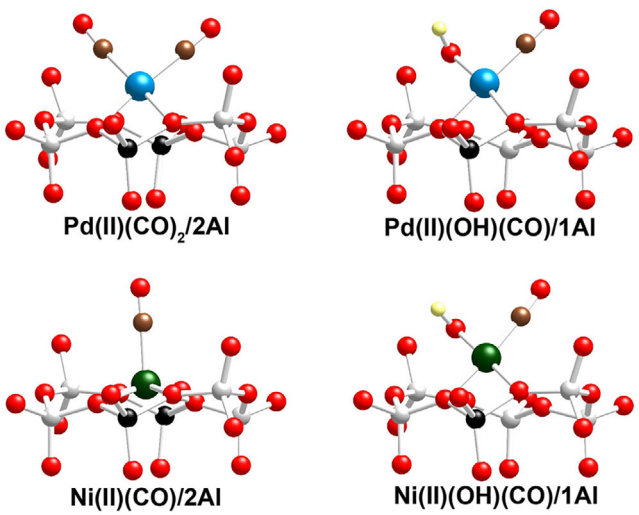

Figure 3. Local structure of the modelled carbonyl complexes. Color coding: Si–gray, O–red, Al–black, H–yellow, Pd–blue, and Ni–green.

$[Ni^{+2}(OH)(CO)]^{+1}$/1Al (Figure 3, Table 1). Our results for the complexes of Pd and Ni divalent cations showed that the calculated C─O vibrational frequencies are lower by -58 to -94 cm^{-1} than the experimental bands when PBE + D2 was employed. Similar significant discrepancies were found by us for the $Pd^{+2}(CO)_2$/2Al in CHA zeolite using PW91 + D2.[10] On the contrary, the calculated frequencies with HSE06 are much closer to the experimental data, as the differences in the calculated and experimental frequencies are 2 to -11 cm^{-1}. The calculated frequencies for the monocarbonyl complexes of $[M^{+2}\text{-}OH]^{+1}$/1Al species with both functionals are in line with experimental bands, as the differences are up to 13 and 19 cm^{-1}, respectively, for the calculations performed with PBE + D2 and HSE06.

Thus, in agreement with DFT calculations that predict very significant CO downshift for Pd^{+2} versus $Pd^{+2}(OH)$ (in which OH group is covalently bonded to Pd), we observe the formation of $Pd(II)(CO)_2$ versus Pd(II)(OH)(CO) complex in zeolites. Loading similar Pd amounts in these two H-BEA samples with similar Si/Al ratios thus yields selectively either Pd^{+2}/2Al or $[Pd^{+2}(OH)]^{+1}$/1Al species. This is obviously due to different Al distribution in the same parent H-BEA: for H-BEA prepared in the OH media, paired Al sites are present in abundance to allow for the formation of isolated M^{+2} ions; on the other hand, the F media favors isolation of Al sites, leading to different divalent metal species that have to have an OH group covalently bound to the divalent metal cation to balance the charge. The same applies to Ni ions: $Ni^{+2}(CO)$/2Al shows a band ~ 2210 cm^{-1}, whereas $[Ni^{+2}(OH)(CO)]^{+1}$/1Al adsorbs CO forming the Ni hydroxo monocarbonyl complex with a significantly downshifted CO IR signature at ~ 2132 cm^{-1}.

Table 1: Experimental and calculated C—O vibrational frequencies, $\nu(C–O)^{exp}$ and $\nu(C–O)^{calc}$ in cm^{-1} and difference between calculated and experimental $\nu(C–O)$ frequencies ($\Delta\nu = \nu^{calc}$-ν^{exp}).

Structure	$\nu(C–O)^{exp}$	$\nu(C–O)^{calc}$	$\Delta\nu$	$\nu(C–O)^{calc}$	$\Delta\nu$
		PBE + D2	PBE + D2	HSE06	HSE06
Pd(II)$(CO)_2$/2Al	2192; 2213	2119; 2155	−73; −58	2181; 2208	−11; −5
Pd(II)(OH)(CO)/1Al	2127	2131	4	2146	19
Ni(II)(CO)/2Al	2211	2117	−94	2213	2
Ni(II)(OH)(CO)/1Al	2132	2119	−13	2145	13

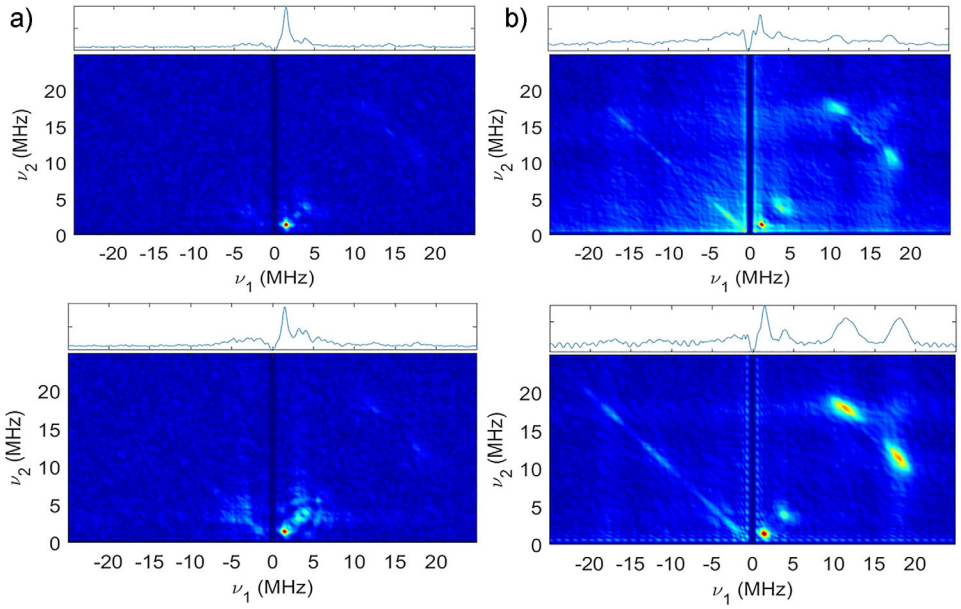

Figure 4. HYSCORE spectra of dehydrated 1 wt% Cu/H-BEA collected at 5 K. a) Cu/H-BEA (OH) upper 3350 G, lower 3420 G. b) Cu/H-BEA (F) upper 3270 G, lower 3370 G. Cu/H-BEA(F) samples show strong coupling to nearby protons (~14.6 MHz on the diagonal). Echo Detected field swept spectra with the HYSCORE positions marked are shown in Figure S4.

2D Hyscore Electron Paramagnetic Resonance Reveals the Presence of OH Ligand on Cu Ions in H-BEA (F) and Absence of OH on Cu Ions in H-BEA (OH)

Pd^{+2} and Ni^{+2} are diamagnetic, which precludes their evaluation with EPR techniques. However, Cu^{+2} is paramagnetic and can be assessed with EPR: advanced 2D EPT techniques allow to probe the presence of NMR-active nuclei around Cu. We collected HYSCORE spectra of two dehydrated (Figures S4 and S5) samples of BEA with a copper loading of 1% (Figure 4). Pulsed electron paramagnetic resonance (EPR) of Cu^{+2} centers at 5 K can detect coupling to nearby NMR-active nuclei such as 27Al and 1H. Previous studies have identified both equatorial H2O[41] and proximal and distant hydroxyls.[42–45] Figure 3 shows that when dehydrated, Cu^{+2} in B-BEA (OH) regular sample shows no evidence of strongly coupled protons near Cu (though distant proton can be identified in ESEEM spectra, not shown. Conversely, the spectra of the H-BEA (F) preparation show strong proton coupling that can be identified as originating from proximal hydroxyls in Figure 4. (The corresponding echo detected field swept EPR spectra of dehydrated 1 wt% Cu in H-BEA samples as well as regular in situ CW-EPR spectra of original samples and samples in-situ dehydrated are shown in Figures S4 and S5; EXAFS data for the Cu/BEA samples provide evidence for the mononuclear nature of copper in Figure S6 and Table S2). Thus, EPR provides the direct evidence of presence of the OH group bound to copper ions. This generalizes the findings for other divalent metal cations, such as Pd and Ni, and reveals that divalent metal cations in H-BEA (F) are present as $[M^{+2}(OH)]^{+1}$/1Al species, whereas those in H-BEA (OH) are present are M^{+2}/2Al complexes. The reason behind this is the different framework Al siting in the H-BEA prepared via these two different routes. In H-BEA (F) the Al sites must be sufficiently isolated, whereas in H-BEA (OH) the sufficiently high amount of Al paired sites is present, affording M^{+2}/2Al. Thus, the markedly different Al distribution in these H-BEA crystals with similar Si/Al ratios allowed us for the first time to prepare either M^{+2}/2Al or $[M^{+2}OH]^{+1}$/1Al species in the micropores of H-BEA with the similar Si/Al ratio. See the discussion below regarding the DFT-calculated stabilities of different M(II) and M(II)-OH complexes in H-BEA.

Table 2: Relative energies for each series of M(II)(H_2O) and M(II)(OH) complexes (M=Cr, Ni, Cu, Pd, Pt), ΔE in kJ mol^{-1}, binding energies of the water molecule in the M(II)(H_2O) complexes, BE in kJ mol^{-1}, selected distances in pm and number of unpaired electrons, Ns.

Structure	ΔE	BE (H_2O)	d(M-O_{zeo})	d(M-O(H_2O/OH))	Ns
Cr(II)(H_2O)/2Al	0	–61	203; 204; 205; 207	233	4
Cr(II)(OH)/2Al_H	166		206; 207	182	4
Ni(II)(H_2O)/2Al	0	–77	201; 202; 207; 209	203	2
Ni(II)(OH)/2Al_H	123		205; 210; 214	178	2
Cu(II)(H_2O)/2Al	0	–56	198; 198; 204; 206	224	1
Cu(II)(OH)/2Al_H	121		199; 200	178	1
Pd(II)(H_2O)/2Al	0	–27	205; 205; 208; 210	287	0
Pd(II)(OH)/2Al_H	148		211; 215	191	0
Pt(II)(H_2O)/2Al	0	–18	205; 206; 208; 208	321	0
Pt(II)(OH)/2Al_H	153		207; 209	188	0

DFT Comparison of Stability of M(II)(H_2O) and M(II)(OH) Complexes

M(II)(H_2O) and M(II)(OH) (M=Cr, Ni, Cu, Pd, Pt) complexes were modeled in a six-membered ring of the H-BEA zeolite containing two Al centers. One of the Al centers was compensated by a proton in the case of M(II)(OH). The M(II)(H_2O)/2Al species are more energetically favorable compared to the M(II)(OH)/2Al_H for all considered cations by 121 to 166 kJ mol^{-1} (Table 2, Figure S7). The binding energy of the H_2O varies from −18 kJ mol^{-1} for the Pt(II)(H_2O)/2Al complex to −77 kJ mol^{-1} for the Ni(II)(H_2O)/2Al structure (Table 1). Hence, its exothermicity is much lower than that of the M(H_2O) formation via proton migration from a basic zeolite O center to the O center of the M(OH) species. These results imply that the M(II)(OH) species are unstable in the vicinity of zeolite protons and will be easily converted first to M(II)(H_2O) and after water desorption to M^{+2}. Thus, M(II)(OH) species can be stabilized only at isolated Al centers or when M(II)(OH) species are farther from zeolite Brønsted acidic sites.

Reactivity of 1 wt% Cu/H—BEA Samples with Cu versus Cu—OH Sites in Selective Catalytic Reduction (SCR) of NO

We can now directly compare the reactivity of [Cu^{+2}(OH)]$^{+1}$/1Al versus Cu^{+2}/2Al complexes species in the same zeolite with similar Si/Al ratio (Figure 5; Figure S8). This is important because previously these two different species for Cu ions were generated only in zeolites with different Si/Al ratios, making direct comparison for selective catalytic reduction of NO not straightforward, as Bronsted acid sites concentrations that are the direct participants of catalysis were different.[46] We compared them under the typical industrially relevant SCR conditions.[47] Note that under these conditions, the "seagull" profile related to the transition of the rate-determining step of SCR from binuclear to mononuclear copper catalytic mechanism (typically observed between 300 to 400 ^{0}C in the kinetic regime) is not well resolved at industrially relevant GHSV.[47] Notably, we found that [Cu^{+2}(OH)]$^{+1}$/1Al is more active for selective catalytic reduction (SCR) of nitric oxide with ammonia at the same Cu loading level of 1 wt%. Its reactivity is higher than that of Cu^{+2}/2Al in the temperature range 150 – 400 ^{0}C. Even after subjecting this material to extremely harsh hydrothermal aging at 850 ^{0}C at 3 h in air/10% H_2O flow, the [Cu^{+2}(OH)]$^{+1}$/1Al still maintains its activity, whereas the Cu^{+2}/2Al lost most of its low temperature activity (Figure 5). Thus, we can confirm the difference in redox activity of [Cu^{+2}(OH)]$^{+1}$/1Al versus Cu^{+2}/2Al.

Furthermore, it is known that Cu/Zeolites are active for aerobic methane oxidation in the presence of steam.[5,6,48] The active sites are hypothesized to be di and/or polymeric Cu oxo species. However, one recent computational investigation suggested that [Cu^{+2}(OH)]$^{+1}$/1Al could serve as a catalytically active site for methane conversion to methanol.[48]

Our newly developed synthetic platform provides an opportunity to investigate the catalytic reactivity of both sites. [Cu^{+2}(OH)]$^{+1}$/1Al (Table S3) produced >3 times more methanol than Cu^{+2}/2Al, suggesting that it is indeed catalytically active for selective methane oxidation to methanol (Table S3), whereas Cu^{+2}/2Al is inactive.

Comparison of NO Adsorption Performance of Pd in H-BEA Adsorbents

Pd/Zeolites are employed as passive NO*x* adsorbers (PNAs) under industrially relevant conditions of vehicle exhaust to trap NOx during cold start. The key aspect of comparison of [Pd^{+2}(OH)]$^{+1}$/1Al versus Pd^{+2}/2Al. NO adsorption performance of these adsorbents has been missing. Now, we can clarify it by directly comparing the PNA performance of these two samples with different speciation of Pd. We indeed find that NO adsorption for [Pd^{+2}(OH)]$^{+1}$/1Al versus Pd^{+2}/2Al reveals profound differences: NO release peak temperature is different (Figure 6a). [Pd^{+2}(OH)(NO)]$^{+1}$/1Al complexes release NO at higher temperature than Pd^{+2}(NO)/2Al complexes, thereby providing an opportunity to tune the NO release temperature by changing the Pd speciation. These new results provide the missing understanding for an important class of industrially relevant NO adsorbent Pd/Zeolite materials, highlighting the differences between the adsorption/desorption performance of two different Pd species.

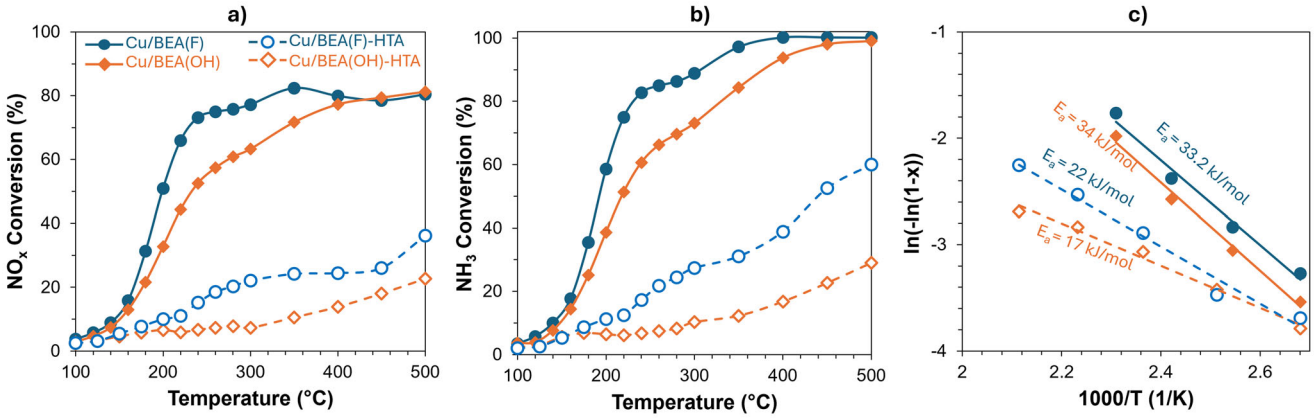

Figure 5. a) SCR activity, b) ammonia conversion, and c) the corresponding Arrhenius plots (at conversion below 20%) for 1 wt% Cu/H-BEA samples (F) and (OH), respectively. Conditions: 365 ppm NO, 365 ppm NH_3, 10% O_2, 3% H_2O, 150 000/h SV, 100 mg catalyst. Hydrothermal aging conditions (severe hydrothermal aging): 850 ^{0}C, 3 h, 10% H_2O/Air at 150 000/h SV.

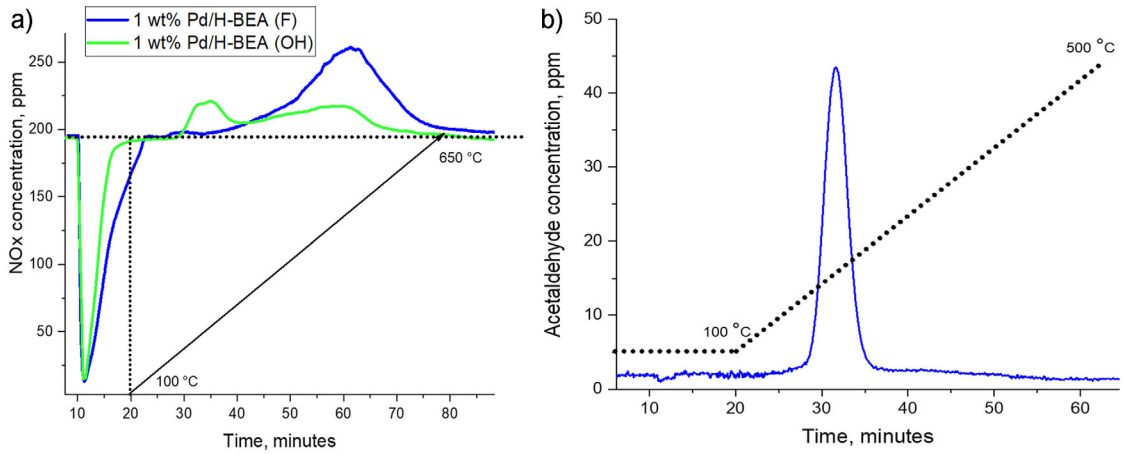

Figure 6. a) NO adsorption at 100 °C for 10 min (after 10 min bypass) followed with TPD (10 °C min^{-1}) for 1 wt% Pd supported on two H-BEA samples. The feed gas mixture contains ~200 ppm of NO, 14% O_2, 200 ppm CO, 3.0% H_2O balanced in nitrogen. GHSV ~ 150 L/g*hr b) Acetaldehyde evolution profile during adsorption at 100 °C for 10 min (after 10 min bypass) followed with TPD (10 °C min^{-1}) for 1 wt% Pd supported on H-BEA (F). The feed gas mixture contained ~ 100 ppm C_2H_4, ~100 ppm of NO, 14% O_2, 3.0% H_2O balanced in nitrogen. GHSV ~ 150 L/g*hr.

Ethene Dimerization and Wacker Oxidation on $[M^{+2}(OH)]^{+1}$/1Al and M^{+2}/2Al Species

Mononuclear $[M^{+2}(OH)]^{+1}$/1Al complexes are fundamentally important materials in catalysis. It is expected that the OH ligands possess unusual reactivity when coordinated to late transition metals because there are no suitable empty orbitals to accept π-electron density from very basic electron pairs on oxygen. This provides a unique opportunity to compare ethylene dimerization activity in these materials. Ethene oligomerization is of importance for catalysis but detailed mechanism insights on heterogeneous catalysts remained obscure until recently.[40] Well-resolved molecular snapshots of the ethylene dimerization demonstrated reactivity on isolated d^8 Ir(I) cations in FAU zeolite.[40] Coordinative unsaturation of metal (super-electrophilic nature of M^{+2}/2Al metal cations in zeolite was recently described in our prior studies)[10] leads to high affinity for the electron density of the C–H bonds, leading to oxidative addition of ethylene with the formation of metal vinyl hydride; this leads to the increase of the oxidation state of the metal by two due to presence of two anionic ligands (hydride and vinyl).[40]

We note that prior reports failed to provide unambiguous mechanistic evidence for this reaction. For example, it was suggested that grafted $[Ni^{+2}(OH)]^{+1}$/1Al sites in Al MCM-41 are active for ethylene dimerization.[49] However, the CO adsorption for the Ni/MCM-41 catalyst produced a CO complex of Ni(II) with a stretching frequency of ~2200 cm^{-1} as a major carbonyl band. As demonstrated in the present study, the presence of OH ligand on Ni or Pd downshifts the CO band of $[Ni^{+2}(OH)(CO)]^{+1}$/1Al complex below that of the gas-phase CO (~2143 cm^{-1}). Thus, the ~2200 cm^{-1} band previously observed after CO adsorption on Ni(II)/MCM-41 zeolite is inconsistent with the conclusion that the material was prepared with the major $[Ni^{+2}(OH)]^{+1}$/1Al species and are indicative of the ~2200 cm^{-1} Ni-CO feature of a $Ni^{+2}(CO)$/2Al complex.[40] Therefore, the competence of $[Ni^{+2}(OH)]^{+1}$/1Al sites in ethene dimerization is primarily

Table 3: Comparison of initial C_4 TOF for Metal/H-BEA. 30 mg catalyst, ethylene flow rate 10 sccm at 1 atm at 100 °C.

Sample	Initial C_4 TOF (min^{-1} per metal atom) at 100 ^0C
1 wt% Pd(II)/BEA	0.67
1 wt% Pd(II)(OH)/BEA (F)	1.55
0.4 wt% Ni(II)/BEA	0.53
0.4 wt% Ni(II)(OH)/BEA(F)	1.33
0.75% wt% Pt(II)/BEA	0.20
0.75 wt% Pt(II)/BEA (F)	0.31
0.3 wt% Cr(II)/BEA	0
0.3 wt% Cr(II)/BEA (F)	0.15

supported by theory since Ni^{+2}/2Al is likely the species responsible for the observed reactivity in that sample.[49]

The present catalytic materials formed dimers (butenes) for both 1Al- and 2Al-supported metal cations at 100 ^0C (Table 3). Notably, $[Pd^{+2}(OH)]^{+1}$/1Al species was ~2.5 times more active for C_4 species formation. This suggests that both sites are active for ethylene dimerization and experimentally proves that $[Pd^{+2}(OH)]^{+1}$/1Al serves as an active site for C_4H_8 formation from C_2H_4 with even higher reactivity than Pd^{+2}/2Al. Similar results were obtained for Ni (Table 1): $[Ni^{+2}(OH)]^{+1}$/1Al sites are also more active for C_4 product formation than Ni^{+2}/2Al. (Table 3).

Different Pd speciation likely indicates different mechanism for C_4 formation on each material; recently, the full mechanistic details of ethylene oligomerization on a heterogeneous catalyst with bare metal ions have been shown,[40] i.e., isolated Ir(I) d^8 ions were shown to start oligomerization cycle through oxidative addition of C–H bond of ethylene to Ir(I) center, with the formation of Ir(III) vinyl hydride, followed by ethylene addition step with the formation of Ir(III) vinyl ethyl complex. Ir(III) vinyl ethyl complex eliminates butenes via reductive elimination.

We can now suggest the following mechanism for ethylene dimerization on $[M^{+2}(OH)]^{+1}$/1Al sites (distinctly different than the mechanism on M^{+2}/2Al):

$$M(II)-OH+2C_2H_4 \longleftrightarrow C_2H_4\text{–}M-OH\text{–}C_2H_4 \longleftrightarrow$$
$$[C_2H_4\text{—}M(II)-O-C_2H_5] \longleftrightarrow$$
$$[M(II)-O-C_4H_9] \rightarrow M(II)-OH+C_4H_8 \quad (1)$$

In this case, the divalent metal does not undergo oxidation change. This agrees with the recent theoretical work that assessed this mechanism for $[M^{+2}(OH)]^{+1}$/1Al sites in BEA zeolite with DFT calculations.[50]

We note that our study represents the first example where isolated $[M^{+2}(OH)]^{+1}$/1Al and M^{+2}/2Al sites were constructed on an identical support and directly compared. We reveal that both sites are catalytically active, with the higher activity of $[M^{+2}(OH)]^{+1}$/1Al for ethylene dimerization.

Furthermore, we also prepared Pt/H-BEA. To the best of our knowledge, Pt/zeolites were not evaluated or shown to have activity in olefin di- and oligomerization (Table 3). We find that both Pt sites in H-BEA are catalytically active for ethylene dimerization. Interestingly, similarly to Pd and Ni, $[Pt^{+2}(OH)(CO)]^{+1}$/1Al shows higher activity than Pt^{+2}/2Al. Thus, our findings are consistent across a range of d^8 metal cations in zeolites.

This now allows us to further provide a new mechanistic insight into one of the most important organic reactions, which is Wacker oxidation of ethylene to acetaldehyde.[51] This deceitfully simple reaction proved extremely elusive to draw a mechanism because Pd(II) complexes in water/solution that catalyze it are notoriously inhomogeneous and hard to characterize.[51,52] Different mechanistic suggestions culminated in two different mechanistic proposals: in one, the direct presence of OH group on Pd(II) is required (the inner sphere mechanism). In the other one, Pd(II) does not require presence of OH group as the external/outer-sphere attack comes from hydroxide in water. Importantly, our system allows us to test this prediction. Experiments (Figure 6b) were performed in the presence of NO; as we recently demonstrated, the role of NO in Pd(II)/Zeolites is to prevent its reduction by simple reductants (such as CO, olefins).[53] The Cu,Pd in zeolite systems rely on sacrificial Cu(II) to re-oxidize Pd(0) to Pd(II),[51,52] similar to our system in which gas phase NO preserves cationic Pd.[53,54] Without NO, Pd is easily reduced in zeolite in the presence of moisture and reductant.[33,34] $[Pd^{+2}(OH)]^{+1}$/1Al sample produced significant amount of acetaldehyde during ethylene oxidation (Figure 6b). In contrast, Pd^{+2}/2Al rich sample did not lead to formation of acetaldehyde above 10 ppm. Therefore, we reveal the aspects of Wacker chemistry that were not possible to obtain using homogeneous complexes; this result suggests that the OH group on Pd^{+2} is beneficial to observe Wacker oxidation (Figure 5b).

We may suggest the following reaction scheme:

$$[Pd^{+2}(OH)]^{+1}/1Al + C_2H_4 \rightarrow [Pd^{+2}(OH)(C_2H_4)]^{+1}/1Al \rightarrow$$
$$[Pd^{+2}(CH_2CH_2OH)]^{+1}/1Al \rightarrow [Pd^{+2}H]^{+1}/1Al + CH_3CHO \quad (2)$$

Evaluation of Mechanistic Proposals for Ethene Dimerization Catalysis by DFT

The formation of 1-butene on $[M^{+2}(OH)]^{+1}$/1Al species was modeled via two reaction mechanisms starting with the adsorption of two ethene molecules, which is a strongly exothermic step by 111 ÷ 161 kJ mol^{-1} on Cr(II), Cu(II), and Ni(II) sites and more than 240 kJ mol^{-1} on Pd(II) and Pt(II) sites. This indicates that C_2H_4 binds approximately twice as strongly to palladium and platinum metal cations than to the other metal cations considered. The next step in the first reaction scheme is the formation of an ethoxy group, which is energetically favorable by 46–64 kJ mol^{-1} (Table 4, Figure 6, reaction scheme 1). The interaction of the ethoxy group with the second ethene molecule leads to the formation of a butoxy group and is exothermic by 22, 47, and 67 kJ mol^{-1} on the Ni(II), Cr(II), and Cu(II), respectively and endothermic by 73 and 125 kJ mol^{-1} on Pd(II) and Pt(II), respectively. The desorption of the butene molecule is strongly unfavorable by around 100 kJ mol^{-1}. The

Table 4: Reaction energies in kJ mol^{-1} of the modelled mechanisms—Scheme 1: $M(II)(OH) + 2C_2H_4 \rightarrow M(II)(OH)(C_2H_4)(C_2H_4) \rightarrow M(II)(OC_2H_5)(C_2H_4) \rightarrow M(II)(OC_4H_9) \rightarrow M(II)(OH) + C_4H_8$; Scheme 2: $M(II)(OH) + 2C_2H_4 \rightarrow M(II)(OH)(C_2H_4)(C_2H_4) \rightarrow M(II)(OH)(C_4H_8) \rightarrow M(II)(OH) + C_4H_8$; Scheme 3: $M(II)/2Al + 2C_2H_4 \rightarrow M(II)(C_2H_4)_2/2Al \rightarrow M(II)(CH_2CH_2CH_2CH_2)/2Al \rightarrow M(IV)(H)(C_4H_7)/2Al \rightarrow M(II)/2Al + C_4H_8$.

Reaction[a]	Cr(II)	Ni(II)	Cu(II)	Pd(II)	Pt(II)
Scheme 1					
$M(II)(OH)/1Al + 2C_2H_4 \rightarrow M(II)(OH)(C_2H_4)(C_2H_4)/1Al$[b]	−135	−161	−111	−244	−293
$M(II)(OH)(C_2H_4)(C_2H_4)/1Al$[b] $\rightarrow M(II)(OC_2H_5)(C_2H_4)/1Al$	−46	−59	−50	−61	−64
$M(II)(OC_2H_5)(C_2H_4)/1Al \rightarrow M(II)(OC_4H_9)/1Al$	−47	−22	−67	73	125
$M(II)(OC_4H_9)/1Al \rightarrow M(II)(OH)/1Al + C_4H_8$	99	112	98	103	102
Scheme 2					
$M(II)(OH)/1Al + 2C_2H_4 \rightarrow M(II)(OH)(C_2H_4)(C_2H_4)/1Al$[b]	−135	−161	−111	−244	−293
$M(II)(OH)(C_2H_4)(C_2H_4)/1Al$[b] $\rightarrow M(II)(OH)(C_4H_8)/1Al$	−115	−119	−126	−110	−122
$M(II)(OH)(C_4H_8)/1Al \rightarrow M(II)(OH)/1Al + C_4H_8$	121	150	108	225	285
Scheme 3					
$M(II)/2Al + 2C_2H_4 \rightarrow M(II)(C_2H_4)_2/2Al$	−75	−116	−73	−199	−266
$M(II)(C_2H_4)_2/2Al \rightarrow M(IV)(CH_2CH_2CH_2CH_2)/2Al$	−22	28	14	78	122
$M(IV)(CH_2CH_2CH_2CH_2)/2Al \rightarrow M(IV)(H)(C_4H_7)/2Al$	84	27	44	22	−26
$M(IV)(H)(C_4H_7)/2Al \rightarrow M(II)/2Al + C_4H_8$	−116	−69	−114	−31	41

[a] *The overall reaction energy ($2C_2H_4 \rightarrow C_4H_8$) is* -129 kJ mol^{-1}. [b] The second C_2H_4 molecule is not coordinated to the metal cation, but is weakly bound to the OH group. The structures in which it is bound to the M(II) cation are less stable by 20 to 60 kJ mol^{-1}depending *on the metal cation*.

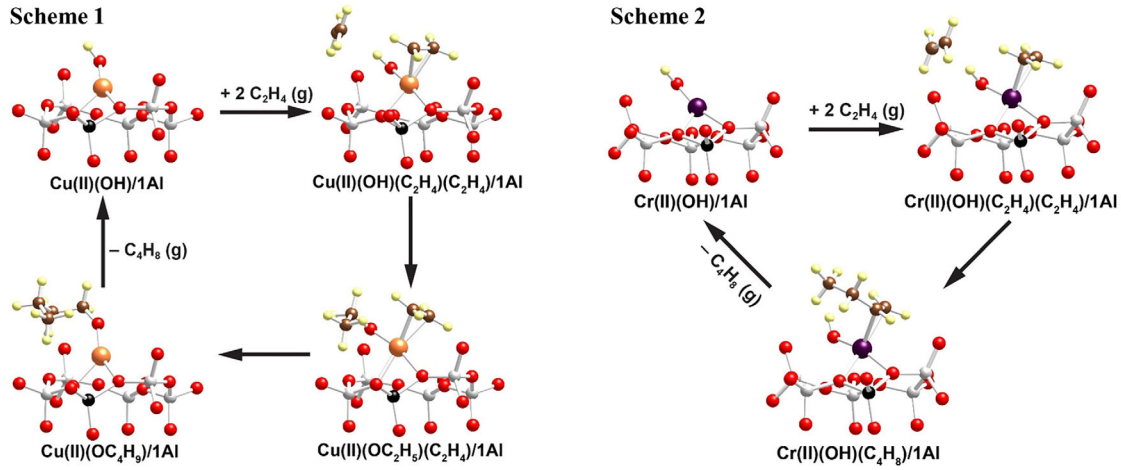

Figure 7. Representation of the reaction mechanisms of Schemes 1 and 2. For visual clarity, the local structure of the complexes located in BEA zeolite is shown. Color coding: Si–gray, O–red, Al–black, H–yellow, and Cr–purple.

second step in the other reaction scheme considered involves a simultaneous transfer of the proton from the OH group to a CH_2 group from one of the C_2H_4 molecules forming a methyl group and a transfer of H from the CH_2 group from the other C_2H_4 molecule, which leads to the formation of $CH_2{=}CH{-}$ moiety and the restoration of the OH group (Table 4, Figure 7, reaction scheme 2). The process is strongly exothermic by more than 110 kJ mol^{-1} on all metal cations and is followed by the desorption of butene. It is endothermic by 108 – 285 kJ mol^{-1} but could be overcome by the adsorption of another two ethene molecules—see the reactions energies of the $[M^{+2}(OH)]^{+1}/1Al + 2C_2H_4 \rightarrow [M^{+2}(OH)(C_2H_4)(C_2H_4)]^{+1}/1Al$ step.

Alternatively, we modeled the formation of butene on $M^{+2}/2Al$ species with no participation of an OH group (Table 4, reaction scheme 3 and Figure 8). The adsorption of two ethene molecules to the $M^{+2}/2Al$ sites is exothermic by 73 ÷ 266 kJ mol^{-1}. The two molecules interact with each other thus forming a $CH_2CH_2CH_2CH_2$ cyclic moiety bound to the metal cation via the two terminal CH_2 groups as the process is energetically favorable by 22 kJ mol^{-1} only in the case of Cr and endothermic by 14–122 kJ mol^{-1} on the other metal cations. Next, an H species is transferred to the metal site thus obtaining $M(IV)(H)(C_4H_7)$ complex, which is also not energetically favorable by 22 ÷ 84 kJ mol^{-1} for Cr, Ni, Cu, and Pd cations and slightly exothermic by 26 for Pt(II). The formation and desorption of butene is exothermic by 31 ÷ 116 kJ mol^{-1} except for Pt(II) cation on which it is energetically unfavorable by 41 kJ mol^{-1}.

From the first two modeled reaction schemes, the second one seems to be more plausible for Pd(II)(OH) and Pt(II)(OH) since only the desorption of butene is endothermic but becomes energetically favorable when is accompanied by the adsorption of new ethene molecules from the gas phase.

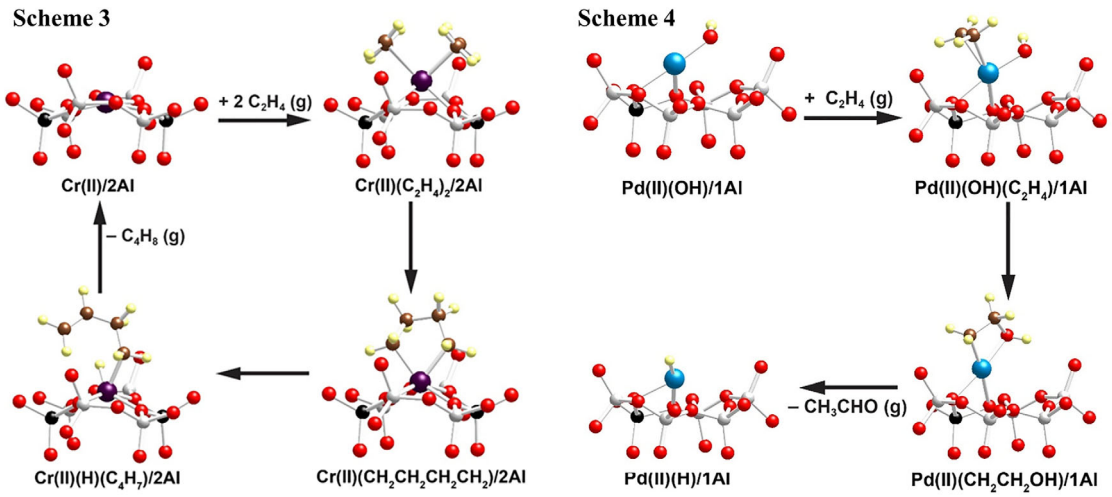

Figure 8. Representation of the reaction mechanisms of Schemes 3 and 4. For visual clarity, the local structure of the complexes located in BEA zeolite is shown. Color coding: Si–gray, O–red, Al–black, H–yellow, Cr–purple, and Pd–blue.

Table 5: Reaction energies, ΔE_{reac} *in kJ* mol^{-1}*of* the modelled mechanism Pd(II)(OH)/1Al + C_2H_4 → Pd(II)(OH)(C_2H_4)/1Al→ Pd(II)(CH_2CH_2OH)/1Al → Pd(II)-H/1Al + CH_3CHO (Scheme 4 in Figure 8).

Reaction	ΔE_{reac}
Pd(II)(OH)/1Al + C_2H_4 → Pd(II)(OH)(C_2H_4)/1Al	−204
Pd(II)(OH)(C_2H_4)/1Al → Pd(II)(CH_2CH_2OH)/1Al	−6
Pd(II)(CH_2CH_2OH)/1Al → Pd(II)-H/1Al + CH_3CHO	182
Overall reaction energy	−28

Additionally, we considered the formation of acetaldehyde from ethene on a $[Pd^{+2}(OH)]^{+1}$/1Al site starting from strongly exothermic adsorption of one C_2H_4 molecule by 204 kJ mol^{-1}, followed by the formation of CH_2CH_2OH species with a slight energy gain of 6 kJ mol^{-1} and formation and desorption of CH_3CHO, which require 182 kJ mol^{-1} (Table 5, Figure 8). However, the overall reaction energy is exothermic by 28 kJ mol^{-1}. In addition, the strong endothermicity of the last reaction step can be compensated by the adsorption of another ethene molecule.

Evaluation of Ethylene Dimerization Reactivity of Cr Zeolite Catalysts with Cr^{+2}/2Al and $[Cr^{+2}(OH)]^{+1}$/1Al Sites

The Phillips catalytic process utilizes grafted Cr ions on silica as active sites for ethylene oligomerization. The specific mechanism is unknown due to the heterogeneity of Cr species present on the surface. Only a fraction of the Cr sites is catalytically active, as recently shown.[55,56] We previously suggested, based on analogies between M ions in zeolites, that ethylene oligomerization may start with the homolytic activation of C–H bonds on highly electrophilic bare Cr sites with the initial formation of Cr vinyl hydride, followed by Cr hydride reaction with ethylene to form ethyl.[40]

Notably, the potential for active Cr-OH sites in olefin activation has not been demonstrated before.

To assess this, 0.3 wt% Cr in H-BEA was formed as each Cr^{+2}/2Al or $[Cr^{+2}(OH)]^{+1}$/1Al sites. Cr^{+2}/2Al was inactive in ethylene di-/oligomerization (Table 3). In contrast, Cr-OH species had measurable activity in ethene dimerization at 100 ^{0}C (Table 3). This suggests that Cr-OH sites grafted on surfaces are active for ethylene oligomerization:

$$(O_{support})_x - Cr - OH + 2C_2H_4 \rightarrow (O_{support})_x - Cr(C_2H_4)$$

$$(OH\text{–}C_2H_4) \rightarrow (O_{support})_x - Cr(C_2H_4)(OC_2H_5) \rightarrow [(O_{support})_x - Cr(O - C_4H_9)] \rightarrow (O_{support})_x - Cr - OH + C_4H_8 \quad (3)$$

This chemistry has not been considered in the Philips oligomerization catalysis literature before, and this new evidence suggests it may be important.

Conclusions

In summary, we provide a synthetic route to intentionally form either M^{+2}/2Al or $[M^{+2}(OH)]^{+1}$/1Al cations in the same zeolite topology with similar Si/Al ratio. A spectroscopic and theoretical framework was used to assess divalent metal speciation in these materials. Their successful synthesis allowed for the elucidation of new mechanistic aspects of industrially and fundamentally important hydrocarbon catalysis, NO adsorption, and SCR. These findings enable a pathway to tune divalent metal ion distributions in zeolites and manipulate activities for adsorption and catalytic reactions.

Acknowledgements

The research described in paper is part of the Quickstarter Initiative at Pacific Northwest National Laboratory. It was conducted under the Laboratory Directed Research and Development Program at PNNL, a multiprogram national laboratory operated by Battelle for the U.S. Department of Energy. The research described in this paper was performed in the Environmental Molecular Sciences Laboratory (EMSL), a national scientific user facility sponsored by the DOE's

Office of Biological and Environmental Research and located at the Pacific Northwest National Laboratory (PNNL). PNNL is operated for the US DOE by Battelle (DE-AC06-76RLO 1830, DE-AC05-RL01830, FW-47319). This work was partially supported by the US Department of Energy (DOE), Office of Science, Office of Basic Energy Sciences (BES), Division of Chemical Sciences, Geosciences, and Biosciences, under the project "Advancing Key Catalytic Reaction Steps for Achieving Carbon Neutrality" (FWP 47319).The authors are grateful for partial support from the Department of Energy; Vehicle Technology office (VTO DOE).IZK is grateful to the European Union-NextGenerationEU, through the National Recovery and Resilience Plan of the Republic of Bulgaria, project No BG-RRP-2.004–0008 for the financial support. HAA gratefully acknowledges the support provided by the project UNITe BG16RFPR002-1.014–0004 funded by PRIDST. The computational resources were provided by Discoverer supercomputer of SofiaTech Park. The authors thank COST Action CA20126 for stimulating the present study.

Conflict of Interests

The authors declare no conflict of interest.

Data Availability Statement

The data that support the findings of this study are available in the Supporting Information of this article.

Keywords: Divalent metal cations in a zeolite · Mechanism of ethylene di- and oligomerization · Philips catalyst · Waker oxidation · Zeolite synthesis

[1] H. Heinemann, *Handbook of Heterogeneous Catalysis*, Wiley-Verlag Chemie, Weinheim, **1997**.
[2] W. M. H. Sachtler, *Acc. Chem. Res.* **1993**, *26*, 383–387, https://doi.org/10.1021/ar00031a005.
[3] A. Finiels, F. Fajula, V. Hulea, *Catal. Sci. Technol.* **2014**, *4*, 2412–2426, https://doi.org/10.1039/C4CY00305E.
[4] K. Khivantsev, M. Derewinski, J. Szanyi, *Microporous Mesoporous Mater.* **2023**, *358*, 112378, https://doi.org/10.1016/j.micromeso.2022.112378.
[5] M. J. Wulfers, S. Teketel, B. Ipek, R. F. Lobo, *Chem. Commun.* **2015**, *51*, 4447–4450, https://doi.org/10.1039/C4CC09645B.
[6] B. Ipek, R. F. Lobo, *Chem. Commun.* **2016**, *52*, 13401–13404, https://doi.org/10.1039/C6CC07893A.
[7] J. Pan, J. Lee, M. Li, B. A. Trump, R. F. Lobo, *J. Catal.* **2022**, *413*, 812–820, https://doi.org/10.1016/j.jcat.2022.07.018.
[8] Y. Yuan, J. S. Lee, R. F. Lobo, *J. Am. Chem. Soc.* **2022**, *144*, 15079–15092.
[9] K. I. Hadjiivnov, G. N. Vayssilov, *Adv. Catal.* **2002**, *47*, 307–511.
[10] K. Khivantsev, N. R. Jaegers, I. Z. Koleva, H. A. Aleksandrov, L. Kovarik, M. Engelhard, F. Gao, Y. Wang, G. N. Vayssilov, J. Szanyi, *J. Phys. Chem. C* **2020**, *124*, 309–321, https://doi.org/10.1021/acs.jpcc.9b06760.
[11] M. Moliner, C. Martínez, A. Corma, *Chem. Mater.* **2014**, *26*, 246–258, https://doi.org/10.1021/cm4015095.
[12] A. Belen Pinar, L. Gomez-Hortiguela, J. Perez-Pariente, *Chem. Mater.* **2007**, *19*, 5617–5626, https://doi.org/10.1021/cm071753o.
[13] T. Yokoi, H. Mochizuki, S. Namba, J. N. Kondo, T. Tatsumi, *J. Phys. Chem C* **2015**, *119*, 15303–15315, https://doi.org/10.1021/acs.jpcc.5b03289.
[14] E. Dib, T. Mineva, E. Veron, V. Sarou-Kanian, F. Fayon, B. Alonso, *J. Phys. Chem. Lett.* **2018**, *9*, 19–24, https://doi.org/10.1021/acs.jpclett.7b03050.
[15] V. Pashkova, S. Sklenak, P. Klein, M. Urbanova, J. Dedecek, *Chem. - Eur. J.* **2016**, *22*, 3937–3941, https://doi.org/10.1002/chem.201503758.
[16] J. Dědeček, D. Kaucký, B. Wichterlová, O. Gonsiorová, *Phys. Chem. Chem. Phys.* **2002**, *4*, 5406–5413.
[17] K. Khivantsev, M. A. Derewinski, L. Kovarik, M. Bowden, X. S. Li, N. R. Jaegers, D. Boglaienko, X. I. Pereira-Hernandez, C. Pearce, Y. Wang, J. Szanyi *Catalysts* **2024**, *14*, 56, https://doi.org/10.3390/catal14010056.
[18] J. Dedecek, Z. Sobalík, B. Wichterlova, *Catal. Rev. Sci. Eng.* **2012**, *54*, 135–223, https://doi.org/10.1080/01614940.2012.632662.
[19] A. B. Pinar, L. Gomez-Hortiguela, J. Perez-Pariente *Chem. Mater.* **2007**, *19*, 5617–5626, https://doi.org/10.1021/cm071753o.
[20] A. Palčić, V. Valtchev, *Appl. Catal. A Gen.* **2020**, *606*, 117795.
[21] S. Park, T. Biligetu, Y. Wang, T. Nishitoba, J. N. Kondo, T. Yokoi, *Catal. Today* **2018**, *303*, 64–70, https://doi.org/10.1016/j.cattod.2017.07.022.
[22] T. Yokoi, H. Mochizuki, T. Biligetu, Y. Wang, T. Tatsumi, *Chem. Lett.* **2017**, *46*, 798–800, https://doi.org/10.1246/cl.170156.
[23] K. Muraoka, W. Chaikittisilp, T. Okubo, *J. Am. Chem. Soc.* **2016**, *138*, 6184–6193, https://doi.org/10.1021/jacs.6b01341.
[24] T. Biligetu, Y. Wang, T. Nishitoba, R. Otomo, S. Park, H. Mochizuki, J. N. Kondo, T. Tatsumi, T. Yokoi, *J. Catal.* **2017**, *353*, 1–10.
[25] K. Muraoka, W. Chaikittisilp, Y. Yanaba, T. Yoshikawa, T. Okubo, *Angew. Chem. Int. Ed.* **2018**, *57*, 3742–3746, https://doi.org/10.1002/anie.201713308.
[26] V. Pashkova, S. Sklenak, P. Klein, M. Urbanova, J. Dedecek, *J. Chem. Eur. J.* **2016**, *22*, 3937–3941, https://doi.org/10.1002/chem.201503758.
[27] J. Holzinger, P. Beato, L. F. Lundegaard, J. Skibsted, *J. Phys. Chem. C* **2018**, *122*, 15595–15613, https://doi.org/10.1021/acs.jpcc.8b05277.
[28] C. Márquez-Alvarez, A. B. Pinar, R. García, M. Grande-Casas, J. Pérez-Pariente *Top. Catal.* **2009**, *52*, 1281–1291, https://doi.org/10.1007/s11244-009-9273-6.
[29] T. Nishitoba, N. Yoshida, J. N. Kondo, T. E. Yokoi, *Chem. Res.* **2018**, *57*, 3914–3922. [Google Scholar].
[30] A. Kharchenko, V. Zholobenko, A. Vicente, C. Fernandez, H. Vezin, V. De Waele, S. Mintova, *Phys. Chem. Chem. Phys.* **2018**, *20*, 2880–2889, https://doi.org/10.1039/C7CP07650A.
[31] E.-P. Ng, X. Zou, S. Mintova, In *New and Future Developments in Catalysis*, S. L. Suib, Ed., Elsevier: Amsterdam, The Netherlands, **2013**, pp. 289–310. ISBN 9780444538765.
[32] V. Pashkova, P. Klein, J. Dedecek, V. Tokarova, B. Wichterlova, *Microporous Mesoporous Mater.* **2015**, *202*, 138–146, https://doi.org/10.1016/j.micromeso.2014.09.056.
[33] V. Gabova, J. Dedecek, J. Cejka *Chem. Commun.* **2003**, 1196–1197, https://doi.org/10.1039/b301634j.
[34] J. Dedecek, V. Balgova, V. Pashkova, P. Klein, B. Wichterlova, *Chem. Mater.* **2012**, *24*, 3231–3239, https://doi.org/10.1021/cm301629a.
[35] A. W. Burton, S. I. Zones, *Stud. Surf. Sci. Catal.* **2007**, *168*, 137–179.
[36] R. F. Lobo, S. I. Zones, M. E. Davis, *J. Inclus. Phenom. Mol.* **1995**, *21*, 47–78, https://doi.org/10.1007/BF00709411.

[37] M. B. Schmithorst, S. Prasad, A. Moini, B. F. Chmelka, *J. Am. Chem. Soc.* **2023**, *145*, 18215–18220, https://doi.org/10.1021/jacs.3c05708.
[38] S. Prodinger, H. Shi, H. Wang, M. A. Derewinski, J. A. Lercher, *Appl. Catal., B* **2018**, *237*, 996–1002, https://doi.org/10.1016/j.apcatb.2018.06.065.
[39] M. A. Camblor, A. Corma, S. Valencia, *J. Mater. Chem.* **1998**, *8*, 2137–2145, https://doi.org/10.1039/a804457k.
[40] N. R. Jaegers, K. Khivantsev, L. Kovarik, D. Klas, J. Z. Hu, Y. Wang, J. Szanyi, *Catal. Sci. Technol.* **2019**, *9*, 6570–6576, https://doi.org/10.1039/C9CY01442J.
[41] C. S. Burns, E. Aronoff-Spencer, C. M. Dunham, P. Lario, N. I. Avdievich, W. E. Antholine, M. M. Olmstead, A. Vrielink, G. J. Gerfen, J. Peisach, W. G. Scott, *Biochemistry* **2002**, *41*, 3991–4001, https://doi.org/10.1021/bi011922x.
[42] S. Maurelli, M. Ruszak, S. Witkowski, P. Pietrzyk, M. Chiesa, Z. Sojka, *Phys. Chem. Chem. Phys.* **2010**, *12*, 10933, https://doi.org/10.1039/c0cp00084a.
[43] P. C. Bruzzese, E. Salvadori, B. Civalleri, S. Jäger, M. Hartmann, A. Pöppl, M. Chiesa, *J. Am. Chem. Soc.* **2022**, *144*, 13079–13083, https://doi.org/10.1021/jacs.2c06037.
[44] A. Wang, Y. Chen, E. D. Walter, N. M. Washton, T. Varga, Y. Wang, J. Szanyi, Y. Wang, C. H. Peden, F. Gao, *Catal. Today* **2021**, *360*, 367–374, https://doi.org/10.1016/j.cattod.2020.01.034.
[45] A. Wang, Y. Chen, E. D. Walter, N. M. Washton, D. Mei, T. Varga, Y. Wang, J. Szanyi, Y. Wang, C. H. Peden, F. Gao, *Nat. Commun.* **2019**, *10*, 1137, https://doi.org/10.1038/s41467-019-09021-3.
[46] M. Signorile, E. Borfecchia, S. Bordiga, G. Berlier, *Chem. Sci.* **2022**, *13*, 10238–10250, https://doi.org/10.1039/D2SC03565K.
[47] F. Gao, D. Mei, Y. Wang, J. Szanyi, C. H. F. Peden, *J. Am. Chem. Soc.* **2017**, *139*, 4935–4942, https://doi.org/10.1021/jacs.7b01128.
[48] Z. Zhao, A. Kulkarni, L. Vilella, J. K. Nørskov, F. Studt, *ACS Catal.* **2016**, *6*, 3760–3766, https://doi.org/10.1021/acscatal.6b00440.
[49] I. Agirrezabal-Telleria, E. Iglesia, *J. Catal.* **2017**, *352*, 505–514, https://doi.org/10.1016/j.jcat.2017.06.025.
[50] N. R. Jaegers, E. Iglesia, *J. Am. Chem. Soc.* **2023**, *145*, 6349–6361, https://doi.org/10.1021/jacs.2c13487.
[51] J. Keith, P. Henry, *Angew. Chem. Int. Ed.* **2009**, *48*, 9038–9049, https://doi.org/10.1002/anie.200902194.
[52] E. W. Stern, *Proc. Chem. Soc.* **1963**, 111.
[53] I. Song, K. Khivantsev, Y. Wang, J. Szanyi, *J. Phys. Chem. C* **2022**, *126*, 1439–1449, https://doi.org/10.1021/acs.jpcc.1c10163.
[54] I. Song, I. Z. Koleva, H. A. Aleksandrov, L. Chen, J. Heo, D. Li, Y. Wang, J. Szanyi, K. Khivantsev, *J. Am. Chem. Soc.* **2023**, *145*, 27493–27499, https://doi.org/10.1021/jacs.3c08916.
[55] D. Trummer, K. Searles, A. Algasov, S. A. Guda, A. V. Soldatov, H. Ramanantoanina, O. V. Safonova, A. A. Guda, C. Copéret, *J. Am. Chem. Soc.* **2021**, *143*, 7326–7341, https://doi.org/10.1021/jacs.0c10791.
[56] Y. Kakiuchi, S. Shapovalova, B. Protsenko, S. Guda, O. V. Safonova, A. Gudab, C. Copéret, *ChemRxiv* **2023**, https://doi.org/10.26434/chemrxiv-2023-9ggbk.

Manuscript received: July 23, 2025
Revised manuscript received: October 01, 2025
Manuscript accepted: October 02, 2025
Version of record online: November 06, 2025